Electronic Supplementary Material (ESI) for Journal of Materials Chemistry B.
This journal is © The Royal Society of Chemistry 2022

Supplementary Information

Zwitterionic silver nanoparticle-incorporated injectable hydrogel with durable and efficient antibacterial effect for accelerated wound healing

*Jun Xiang,[a] Yangjing Bai,[b] Yingchun Huang,[b] Shiying Lang,[a] Juan Li,[c] Ying Ji,[*d] Biyu Peng [a] and Gongyan Liu[*a]*

[a] Key Laboratory of Leather Chemistry and Engineering of Ministry of Education, College of Biomass Science and Engineering, Sichuan University, Chengdu 610065, China.

[b] West China School of Nursing, Sichuan University/Department of Cardiovascular Surgery, West China Hospital, Sichuan University. Chengdu, 610041, China.

[c] CAS Key Laboratory for Biomedical Effects of Nanomaterial & Nanosafety, Institute of High Energy Physics, Chinese Academy of Sciences, Beijing 100049, China.

[d] Institute of Textiles and Clothing, Hong Kong Polytechnic University, Hunghom, Kowloon, Hong Kong SAR.

*Corresponding Author: Ying Ji (E-mail: ying.ji@polyu.edu.hk); Gongyan Liu (E-mail: lgy3506@scu.edu.cn)

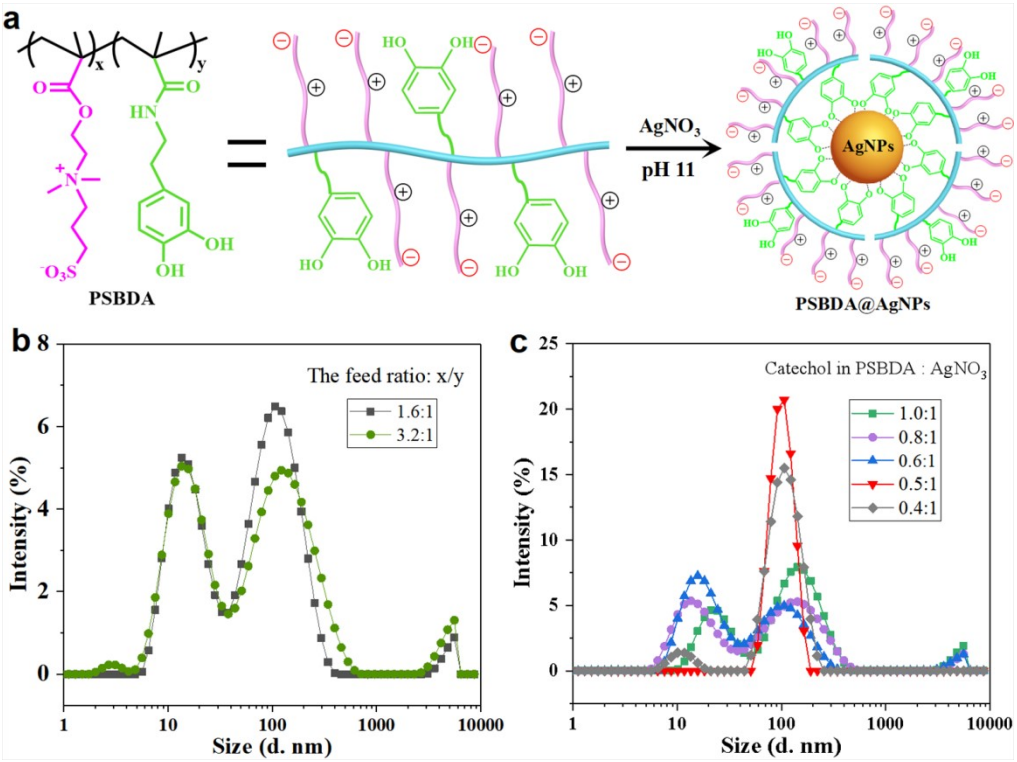

Fig. S1. Optimization of the synthesis of PSBDA@AgNPs by tuning the x/y ratio in PSBDA polymer and the PSBDA/$AgNO_3$ ratio. As demonstrated in the synthetic route in Fig. S1a, the catechol moieties in PSBDA copolymer provided the reducing potential to covert $AgNO_3$ into zero-valence Ag. Meanwhile, the chelation between silver and catechol moieties anchored the PSBDA onto the surface of the as-synthesized AgNPs. The tuning of the ratio between catechol moieties and the sulfobetaine moieties (x/y) in PSBDA and the impact on the size profile of the PSBDA@AgNPs was demonstrated in Fig. S1b. In the cases of PSBDA with x/y ratios of 1.6:1 or 3.2:1, the resulting PSBDA@AgNPs demonstrated two peaks in the DLS size distribution curves, indicating the uniformity of size was not comparable with the PSBDA with an x/y ratio of 2.4:1 (Fig. 1d, main text). Furthermore, the impact of the ratio between PSBDA and $AgNO_3$ in feed was demonstrated in Fig. S1c. Gradient ratios between the catechol groups in PSBDA and $AgNO_3$ were investigated from 1:1 to 0.4:1. Based on the size and distribution, a catechol to $AgNO_3$ ratio of 0.5:1 was identified as the optimized feed ratio, which resulted in PSBDA@AgNPs with the most uniform size distribution. Therefore, the optimized PSBDA@AgNPs for this study were synthesized from PSBDA with an x/y ratio of 2.4:1 and a catechol to $AgNO_3$ ratio of 0.5:1.

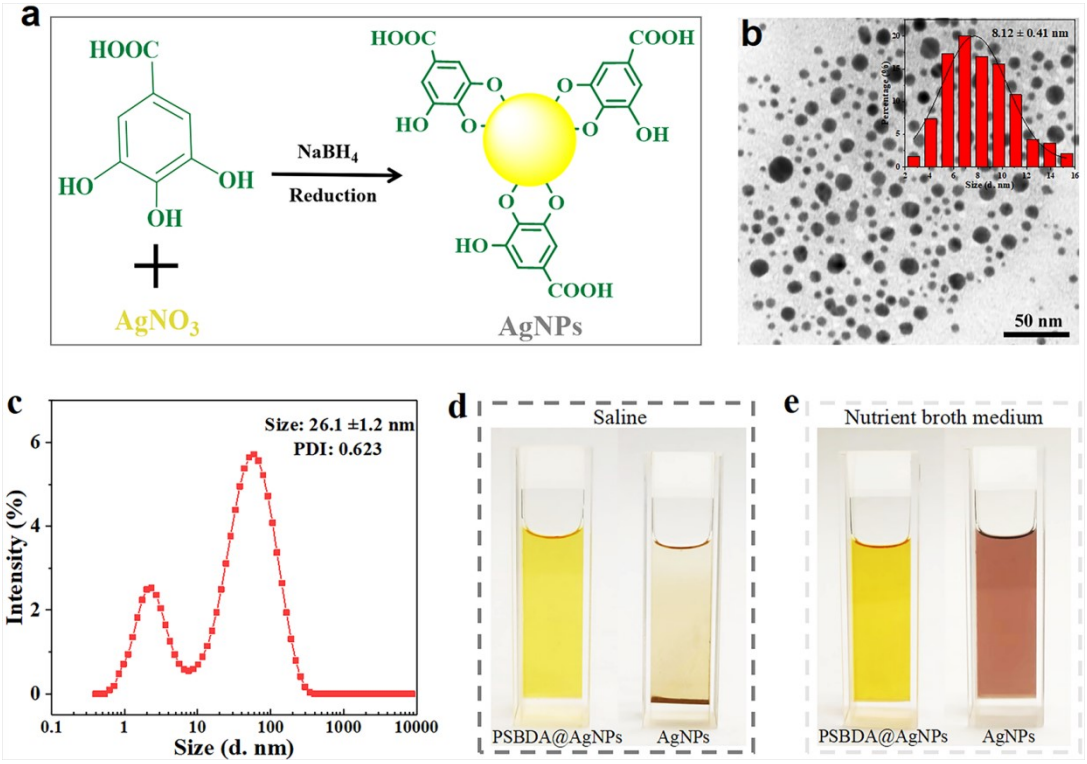

Fig. S2. Synthesis of gallic acid-modified silver nanoparticles (AgNPs) as the non-zwitterionic control for the comparison with PSBDA@AgNPs. As illustrated in Fig. S2a, non-zwitterionic AgNPs were synthesized according to our previous work[1]. Briefly, the aqueous solution of $AgNO_3$ (1.86 mM, 20 mL) and gallic acid (1.86 mM, 20 mL) was first mixed at room temperature. The above mixture was then added dropwise into $NaBH_4$ solution (11.16 mM, 60 mL, 0 °C) under constant stirring, followed by further stirring for 2 h to obtain AgNPs. The TEM morphology of AgNPs was characterized in Fig. S2b and an average TEM diameter of 8.12±0.41 nm was detected. Compared to PSBDA@AgNPs, the non-zwitterionic AgNPs exhibited equivalent average TEM diameter but broader size distribution. The hydrodynamic diameter of AgNPs was characterized in Fig. S2c. Non-zwitterionic AgNPs exhibited an average hydrodynamic diameter of 26.1±1.2 nm and a PDI of 0.623. Compared to PSBDA@AgNPs, gallic acid was less efficient in forming hydration layer onto non-zwitterionic AgNPs and resulted in a smaller hydrodynamic size. The instability of non-zwitterionic AgNPs after incubation with saline and nutrient broth was demonstrated in Fig. S2d and e. Instantly after being dispersed in saline at a silver concentration of 50 ppm, non-zwitterionic AgNPs formed significant aggregates (Fig. S2d). In contrast, PSBDA@AgNPs maintained the yellow color when dispersed in saline at an equivalent concentration (50 ppm). In the case of dispersion in bacterial culture media, the color of non-zwitterionic AgNPs in nutrient broth (50 ppm) instantly turned red (Fig. S2e), which contrasted with the yellowish color when AgNPs were dispersed in water. The color changes indicated the significant size

increase of non-zwitterionic AgNPs in nutrient broth. and the hydrodynamic size was > 1μm with a broad PDI (beyond the reliable detection limit of Zetasizer). In contrast, PSBDA@AgNPs maintained the yellowish color in both saline and nutrient broth (Fig. 1h, i, main text), which suggested a stable size profile.

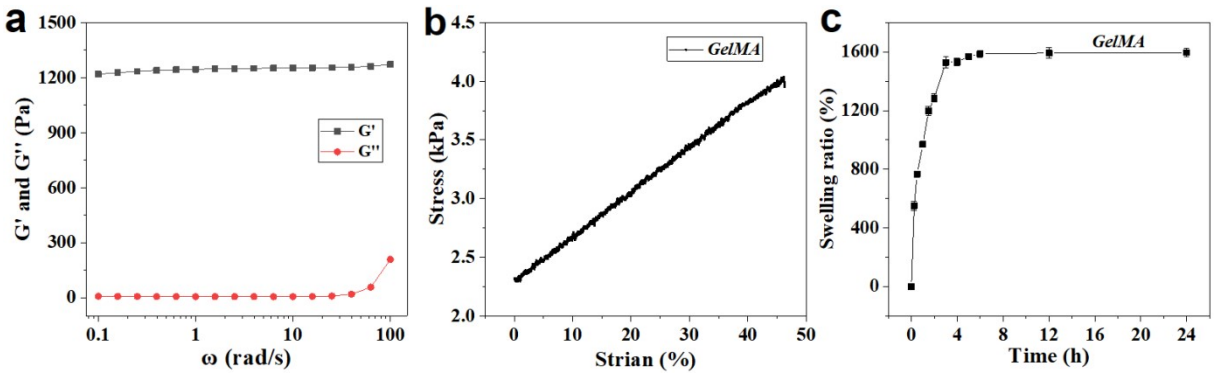

Fig. S3. The mechanical properties and swelling dynamics of single-component GelMA hydrogel. (a) Rheologica characterization of GelMA hydrogel as a function of shear frequency ranging from 0.1 to 100 rad/s. Storage modulus (G′) was constantly greater than the loss modulus (G″), which suggested the elastic characteritistic of GelMA hydrogel. Compared with Fig. 2d (main text), the G′ of single-component GelMA was significantly smaller than PSBDA@AgNPs-GelMA-PVA hydrogel, which indicated that the introduction of PVA component enhanced the strength of the hydrogel. (b) Tensile characterization of GelMA hydrogel (40 mm in length,12 mm in width and 1.8 mm in thickness) at a separation rate of 10 mm/min. The single-component GelMA hydrogel exhibited an elongation at break of 46.25% and a tensile strength of 3.95 kPa. Compared with Fig. 2e (main text), the introduction of PVA in the PSBDA@AgNPs-GelMA-PVA hydrogel enhanced the elasticity and tensile strength of GelMA hydrogel. (c) Swelling profile of GelMA hydrogel indicated a greater swelling ratio compared to PSBDA@AgNPs-GelMA-PVA hydrogel (Fig. 2f, main text).

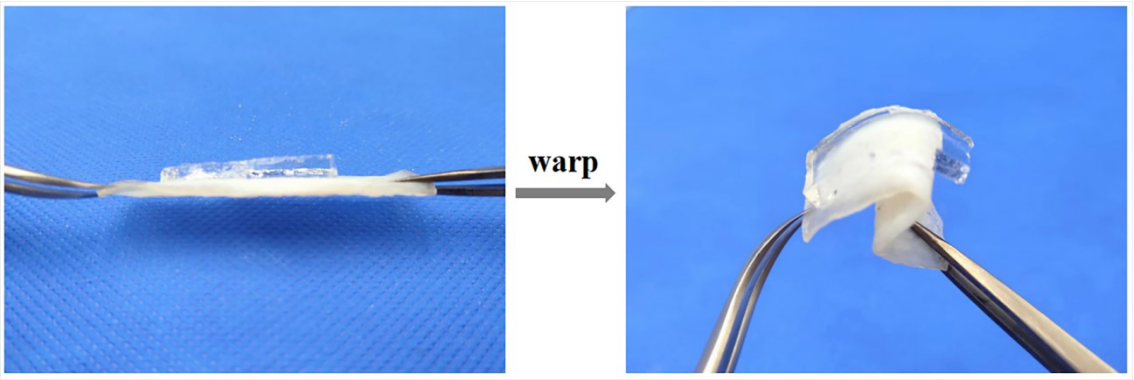

Fig. S4. The low tissue adhesiveness and restricted adaptability of single-component GelMA hydrogel. As demonstrated in the photographs, the GelMA hydrogel (the transparent dressing layer) failed to deform in accordance with the deformation of the pig skin (the white substrate). Compared with the result in Fig. 2g (main text), the introduction of the PVA component enhanced the tissue adhesiveness, flexibility and adaptability of the PSBDA@AgNPs-GelMA-PVA hydrogel.

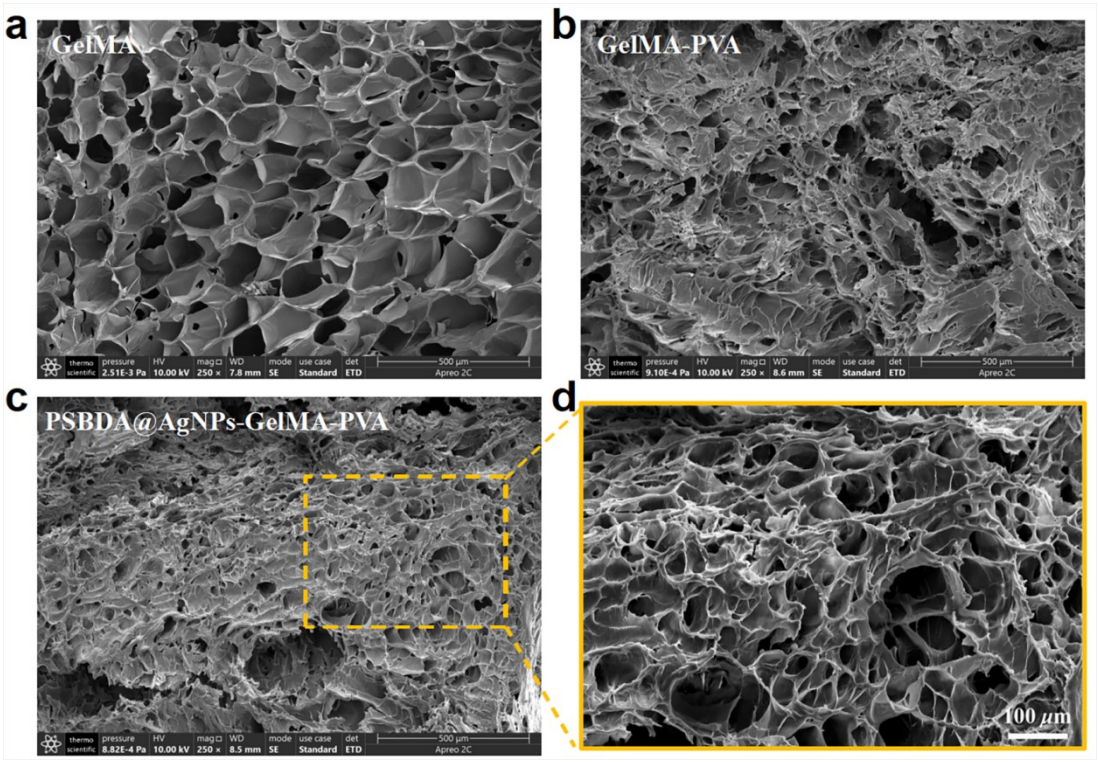

Fig. S5. The SEM morphology of single-component GelMA, blank GelMA-PVA and PSBDA@AgNPs-GelMA-PVA hydrogels. All the hydrogels were formulated at an equivalent concentration of GelMA (5 wt%), PVA (5 wt%) and LAP photoinitiator (0.5% w/w relative to the GelMA content). In the SEM characterization, a relatively greater average pore size was detected in GelMA hydrogel (124.1±7.1 μm). The pore size of blank GelMA-PVA hydrogel was detected as 47.9±2.3 μm, which was equivalent to PSBDA@AgNPs-GelMA-PVA hydrogel (44.1±2.7 μm).

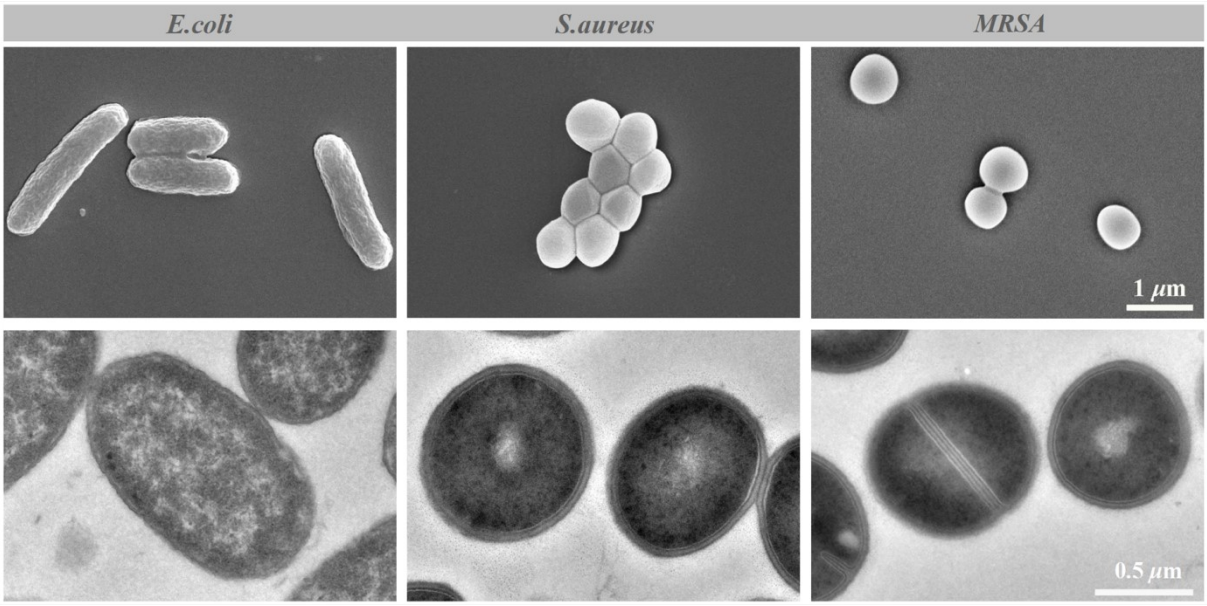

Fig. S6. The morphology of bacteria including *E. coli*, *S. aureus* or *MRSA* after 24 h culture on blank GelMA-PVA hydrogel. Both SEM and TEM characterization indicated intact cell structure of all the three strains of bacteria. The result suggested that blank GelMA-PVA hydrogel did not provide any bactericidal effect.

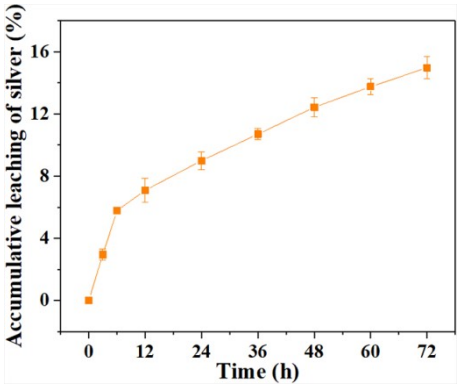

Fig. S7. The release profile of silver from PSBDA@AgNPs-GelMA-PVA hydrogel was studied by inductively coupled plasma atomic emission spectroscopy (ICP-AES, Optima 8000, PerkinElmer, USA). Before the release test, the total silver content of the hydrogel was first determined by ICP-AES. Briefly, PSBDA@AgNPs-GelMA-PVA hydrogel (1g) was solubilized in 10 mL mixed solution of concentrated nitric acid (HNO_3) and H_2O_2 (4:1, v:v) for nitrolysis. The resulting solution was diluted and the silver concentration was determined by ICP-AES. To characterize the release profile of silver, the hydrogel (1g) was placed into 5 mL PBS (pH 7.4) and incubated on an automated shaker (37 ℃, 150rpm). At predetermined time intervals, 5 mL solution was withdrawn and replaced by another 5 mL fresh PBS. The released silver content was then determined by ICP-AES and normalized to the total silver content to calculate the percentage of accumulative release (n=3).

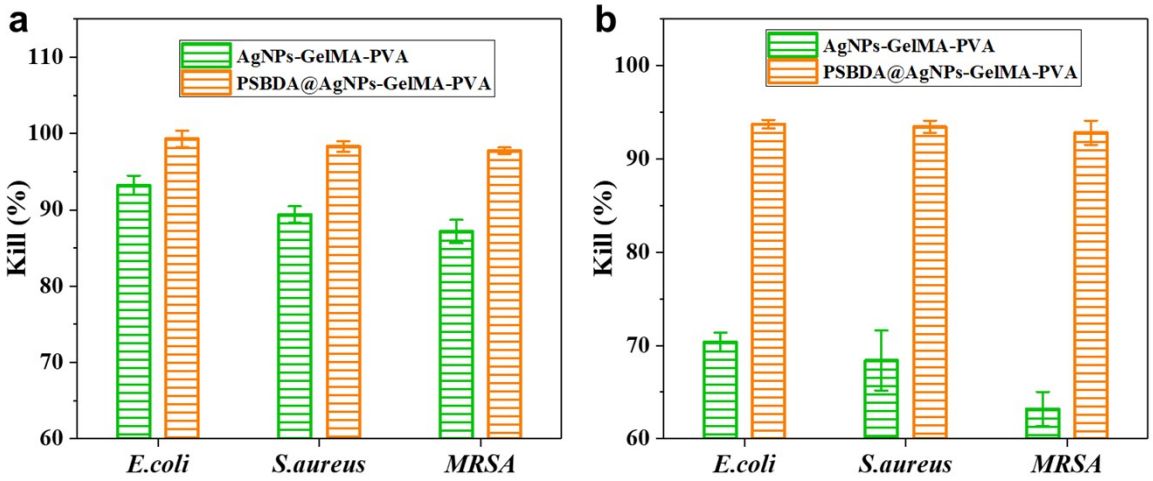

Fig. S8. The bacterial inhibition rate of PSBDA@AgNPs-GelMA-PVA hydrogel in comparison with the non-zwitterionic AgNPs-GelMA-PVA hydrogel, after pre-incubation in (a) saline and (b) nutrient broth for 24 h. Significantly reduced antibacterial efficiency was observed in the non-zwitterionic AgNPs-GelMA-PVA hydrogel after pre-incubation, indicating that both saline and bacterial culture media could impair the colloidal stability of the non-zwitterionic AgNPs and therefore dampened the antibacterial performance. In contrast, persistent bacterial inhibition rate was maintained in PSBDA@AgNPs-GelMA-PVA hydrogel. After incubation with saline, the inhibition rate was detected as 99.31±1.10% for *E. coli*, 98.32±0.71% for *S. aureus, and* 97.76±0.39% for *MRSA*, respectively. After incubation with nutrient broth, the bacterial inhibition rate was detected as 93.76±0.45% for *E. coli*, 93.44±0.67% for *S. aureus,* and 2.81±1.29% for *MRSA*, respectively.

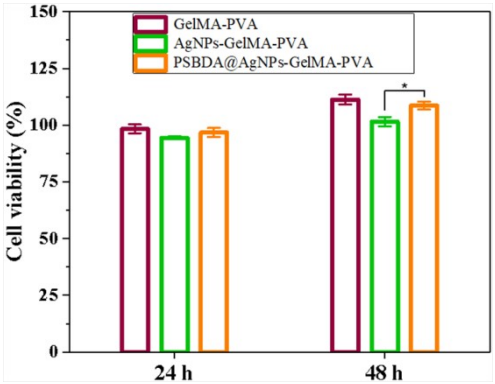

Fig. S9. Biocompatibility of PSBDA@AgNPs-GelMA-PVA hydrogel in HaCaT human keratinocytes. HaCaT cells were cultured on hydrogels for 24 h and 48 h, followed by CCK-8 viability assay. PSBDA@AgNPs-GelMA-PVA did not induce any cytotoxic effect in HaCaT cells (n=3). Statistical significance: *, $p < 0.05$.

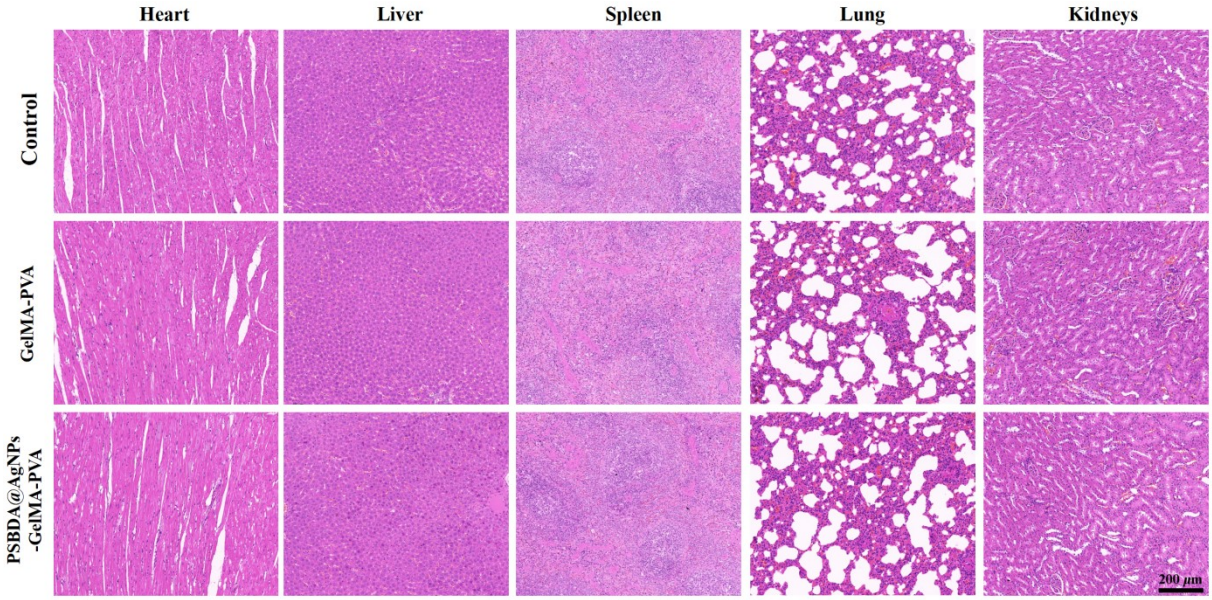

Fig. S10. Histological examination of major organs collected on day 14 of the wound healing test, including heart, liver, spleen, lung and kidneys (scale bar: 200 μm). No histological abnormalities were observed in the major organs of rats treated with PSBDA@AgNPs-GelMA-PVA hydrogel as wound dressing, which indicated the safety and biocompatibility of the hydrogel.

Reference:

1. G. Liu, G. Haiqi, K. Li, J. Xiang, T. Lan and Z. Zhang, *Journal of Colloid and Interface Science*, 2018, **514**, 338-348.